Two-dimensional spatially selective spin inversion and spin-echo refocusing with a single nuclear magnetic resonance pulse

Paul A. Bottomley and Christopher J. Hardy
General Electric Corporate Research and Development Center, P. O. Box 8, Schenectady, New York 12301

(Received 10 March 1987; accepted for publication 6 August 1987)

A new class of nuclear magnetic resonance (NMR) pulses that provides simultaneous spatially selective inversion of nuclear spins in two dimensions following a single pulse application is described and demonstrated. The two-dimensional selective pulses consist of a single square- or amplitude-modulated π rf pulse applied in the presence of an amplitude-modulated magnetic field gradient that reorients through the two dimensions during the rf pulse. For example, square and Gaussian rf pulses produce sharply peaked sombrero-, egg-carton-, and stalagmite-shaped profiles of spin inversion in the xz plane when applied in the presence of a gradient that rotates or describes a figure eight in the xz plane. The theoretical profiles, computed by numerical integration of the Bloch equation, are in good agreement with experimental results obtained by incorporating the pulses into a conventional NMR imaging sequence. The pulses are directly applicable to restricted field-of-view high-resolution imaging for the amelioration of aliasing signal artifacts, and when combined with one-dimensional localized phosphorus (^{31}P) chemical shift spectroscopy techniques that employ surface detection coils, should permit complete three-dimensionally localized ^{31}P NMR spectroscopy. The π pulses provide similar two-dimensional spatial selectivity of the transverse nuclear magnetization when used for refocusing Hahn spin echoes.

I. INTRODUCTION

The selective excitation of nuclear spins in a single spatial dimension by application of a nuclear magnetic resonance (NMR) pulse in the presence of a linear magnetic field gradient constitutes a fundamental and crucial element of most current NMR imaging techniques[1,2] and many spatially resolved spectroscopy methods.[3–5] First proposed by Lauterbur *et al.*[6] and Garroway, Grannel, and Mansfield[7] in 1974, the selective excitation technique has since evolved to include Gaussian,[8] sinc,[9] and sech[10] function amplitude or frequency-modulated NMR pulses to provide Gaussian and square profiled slice selection, and rephasing magnetic field gradient pulses to optimize sensitivity in applications involving $\pi/2$ NMR pulses.[8,11] Yet in all applications of selective excitation that require complete three-dimensional localization of NMR signals in heterogeneous objects, the restriction that these approaches can provide spatial localization in only one dimension each time a selective pulse is applied necessitates the repeated use of gradient and NMR pulses, often in sequences punctuated by the relatively long periods required for the recovery of longitudinal spin magnetization.[1–5]

For example, one three-dimensional chemical shift spectroscopy technique employing selective inversion requires eight different sequence applications consisting of the eight combinations of three orthogonal-pulsed magnetic field gradients with each turned either on or off, and the subsequent addition and subtraction of signals to yield a spectrum from a single fully resolved selected volume element.[4] Should the position of the sample change relative to the gradient fields during this eight-fold sequence application, due to physiological motions during *in vivo* studies, for instance, the signal summation will be in error and the volume localization compromised. Also, in conventional NMR imaging applications, it is often desirable to acquire a high-resolution two-dimensional image restricted to a small region of a much larger sample. However, such imaging attempts by conventional methods are fraught with artifacts produced by excited NMR signals derived from spins that lie outside the region of interest but that are folded back into the picture. Clearly, a selective excitation pulse capable of effecting simultaneous spatial localization in more than one dimension would provide an optimum and much-needed solution to these problems.

We present a technique for providing two-dimensional spatially selective spin inversion or refocusing with a single NMR pulse that is applied in the presence of two spatially orthogonal time-dependent magnetic field gradients. The technique involves rotating the net applied magnetic field gradient direction through the two spatial dimensions in the laboratory frame of reference during the application of a conventional square or an amplitude-modulated NMR π pulse. Different combinations of the time dependence of the gradient reorientation and the modulation of the π pulse produce different spatial sensitivity profiles of the spin inversion and refocusing, with many acceptable and practical solutions available. Although reorienting gradients have previously been applied during the detection of NMR signals for NMR image localization,[12,13] and for localization in chemical shift spectroscopy,[14] their use for selective excitation has, to the best of our knowledge, never been proposed.

II. THEORY

A macroscopically heterogeneous distribution of nuclear spins can be thought of as an array of ensembles of spins

 0021-8979/87/224284-07$02.40

each represented by a bulk nuclear spin magnetization $\mathbf{M}(\mathbf{r})$ at each point $\mathbf{r} = (x,y,z)$ in a laboratory Cartesian coordinate frame of reference. The coordinate system is depicted in Fig. 1. The effect on each ensemble at $\mathbf{r}$ of applying an NMR pulse in the presence of a magnetic field gradient superimposed on a large static magnetic field $H_0\,\hat{z}$ is then given by the Bloch differential equation

$$\frac{d}{dt}\mathbf{M}(\mathbf{r},t) = \gamma \mathbf{M}(\mathbf{r},t) \times \mathbf{H}(\mathbf{r},t) \tag{1}$$

for time t short compared to the spin-spin (T_2) and spin-lattice (T_1) relaxation times, in a local primed frame of reference at $\mathbf{r}$ rotating about an axis parallel to the z axis with angular frequency ω equal to that of the NMR excitation field, denoted by $\mathbf{H}_1(t)$ in the rotating frame. The net applied magnetic field in the rotating frame at $\mathbf{r}$ is

$$\mathbf{H}(\mathbf{r},t) = \mathbf{H}_1(t) + [H_0 + H_g(\mathbf{r},t) - \omega/\gamma]\hat{\mathbf{z}}', \tag{2}$$

where $H_g(\mathbf{r},t)$ is the z component of the applied gradient field, γ is the nuclear gyromagnetic ratio, and $\omega_0 = \gamma H_0 \sim \omega$ is the Larmor angular frequency. Gradients in the x and y components of the magnetic field can be disregarded if their amplitudes in the rotating frame are much less than H_0.[1]

We can compute the net magnetization at the cessation of the NMR pulse for arbitrary NMR pulse and gradient waveforms by numerical integration of Eq. (1) using rotation operators with spherical polar coordinate angles (ϕ,θ) to accommodate the vector product[1] and iterating its differential form

$$\mathbf{M}(t+dt) = R_\phi R_\theta S R_\theta^{-1} R_\phi^{-1} \mathbf{M}(t), \tag{3}$$

commencing with $\mathbf{M}(t=0) = M_0\hat{\mathbf{z}}'$ for spin inversion, where M_0 is the equilibrium magnetization at $\mathbf{r}$, R_θ^{-1} and R_ϕ^{-1} transform the magnetization to a coordinate system in the rotating frame in which the net field $\mathbf{H}$ is directed parallel to the z' axis at $\mathbf{r}$,

$$S = \begin{bmatrix} \cos\alpha & \sin\alpha & 0 \\ -\sin\alpha & \cos\alpha & 0 \\ 0 & 0 & 1 \end{bmatrix}$$

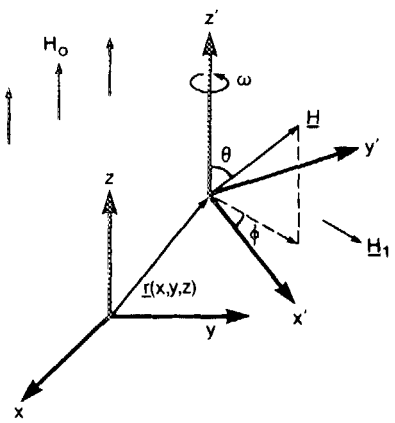

FIG. 1. Coordinate axes used in the theoretical analysis. A local ensemble of nuclear spins in a macroscopically heterogeneous object are located at r (x,y,z) in a laboratory Cartesian coordinate frame immersed in the main static magnetic field $H_0\hat{z}$ and a gradient field $H_g(\mathbf{r})$. The net effective field $\mathbf{H}$ at $\mathbf{r}$ is considered in a primed Cartesian coordinate frame rotating about the z axis at $\mathbf{r}$ with angular frequency $\omega \sim \omega_0$, the NMR transmitter frequency. $\mathbf{H}_1$ is a uniform NMR excitation field in the rotating frame of reference, and (ϕ,θ) cylindrical polar coordinates in that frame.

nutates $\mathbf{M}$ about $\mathbf{H}$ by an increment $\alpha = \gamma H(t)dt$, and

$$R_\theta = \begin{bmatrix} \cos\theta & 0 & \sin\theta \\ 0 & 1 & 0 \\ -\sin\theta & 0 & \cos\theta \end{bmatrix}$$

and

$$R_\phi = \begin{bmatrix} \cos\phi & \sin\phi & 0 \\ -\sin\phi & \cos\phi & 0 \\ 0 & 0 & 1 \end{bmatrix}$$

transform the magnetization back to the original coordinate system with H_0 parallel to the z' axis.

It remains now only to choose suitable forms for $\mathbf{H}_1(t)$ and $H_g(\mathbf{r},t)$. The NMR excitation pulse must be applied transverse to the main H_0 field and may therefore possess two components in the rotating frame. Since these may in general be modulated by different amplitude modulation functions $h_{1x}(t)$ and $h_{1y}(t)$ by means of a quadrature NMR transmitter,[10] we write

$$\mathbf{H}_1 = \hat{\mathbf{x}}' h_{1x}(t) + \hat{\mathbf{y}}' h_{1y}(t). \tag{4}$$

Similarly, for the gradient field we set

$$H_g(\mathbf{r},t) = x g_x h_{gx}(t) + y g_y h_{gy}(t) + z g_z h_{gz}(t), \tag{5}$$

where g_x, g_y, and g_z are the amplitudes of the gradients in the z component of the magnetic field provided by a conventional NMR imaging system employing linear gradient fields, and $h_{gx}(t)$, $h_{gy}(t)$, and $h_{gz}(t)$ are the dimensionless amplitude modulation functions of the respective gradients. The spatial variation or sensitivity profile of the magnetization $\mathbf{M}(\mathbf{r})$ in the laboratory frame produced by a particular NMR pulse and gradient field combination is thus obtained by substituting Eqs. (5), (4), and (2) into (3). The equations are iterated from $t = 0$ to $t = \tau$ at each point (x,y,z) in the array.

A. Sombrero pulse

The simplest example of a two-dimensional spatially selective NMR pulse and gradient field combination obtains for a conventional square π NMR inversion pulse of amplitude h_{10} and duration τ applied in the presence of a gradient field that rotates through 2π in the xz plane, whereby

$$\begin{aligned} &h_{1x}(t) = h_{10} = \pi/\gamma\tau, \quad h_{1y}(t) = 0, \\ &h_{gx}(t) = \sin(2\pi t/\tau), \\ &h_{gz}(t) = \cos(2\pi t/\tau), \quad g_x = g_z, \quad g_y = 0 \end{aligned} \tag{6}$$

for $0 \leqslant t \leqslant \tau$. The resultant sombrero-shaped two-dimensional spatial response profile for the z component of the magnetization is plotted in Fig. 2(a) for a gradient amplitude $g_x = 10^{-3}\,T/m$, a 1-ms pulse length, and a proton (^1H) gyromagnetic ratio. Complete spin inversion is produced along the y axis only at and about the cylindrical axis ($x = 0$, $z = 0$) of the gradient field. Elsewhere, the z magnetization is incompletely inverted or totally unperturbed in a nearly circularly symmetric pattern with the locations of the first few minima at $M_z = M_0$ (no inversion) and sidelobes indicated in the sectional profiles, Fig. 2(b). The half-height widths of the central portion of the response at $M_z = 0$ are approximately given by

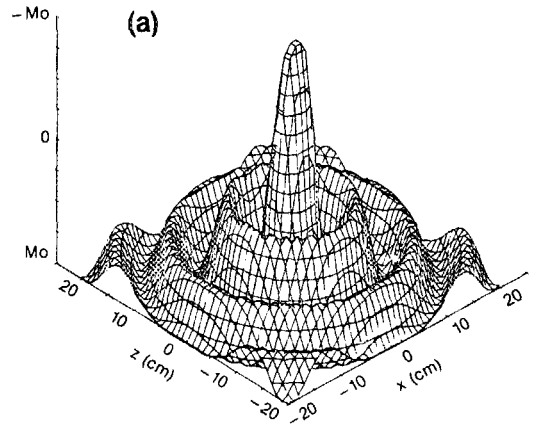

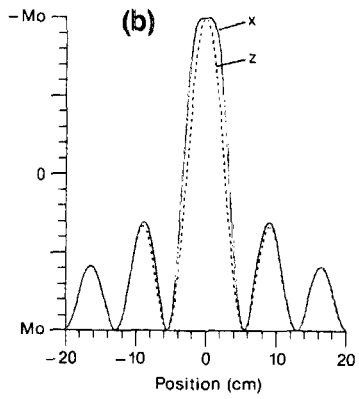

FIG. 2. Computed two-dimensional spatial response of a uniform distribution of nuclear spins subject to a two-dimensional selective NMR inversion pulse defined by Eqs. (6): (a) the sombrero pulse. Vertical axes represent the z component of the nuclear magnetization in units of the equilibrium magnetization M_0 at each point r. Horizontal scales assume $g_x = g_z = 1.0$ mT/m, a ^1H gyromagnetic ratio, and $\tau = 1$ ms. (b) One-dimensional sectional profiles along the x axis (solid curve) and the z axis (dashed curve). The same spatial response for the magnitude of the transverse magnetization is obtained when the sombrero pulse is used for refocusing spin echoes if the range of the vertical axis is rescaled to 0 to M_0 [or $M_0 \exp(-2T_E/T_2)$].

$$\Delta x = 1.8\times 10^4/(\gamma g_x) \text{ m}$$

and

$$\Delta z = 1.5\times 10^4/(\gamma g_z) \text{ m}$$

in the x and z directions, respectively, with gradients in T/m. Thus, the size and shape of the sensitivity profile can be controlled by adjusting the gradient strengths and scale linearly with the gyromagnetic ratio.

B. Egg-carton pulse

The two-dimensional spatial selectivity improves somewhat when a Gaussian amplitude-modulated π pulse is substituted for the square NMR pulse. For example, with

$$h_{1x}(t) = h_{10}\exp(-t^2/2\sigma^2),$$
$$h_{10} = \pi\left[\gamma\int_{-\tau_g}^{\tau_g}\exp\left(\frac{-t^2}{2\sigma^2}\right)dt\right]^{-1} = \frac{\pi}{1.04\gamma\tau_g},$$
$$\tau_g = 2.36\sigma = \tau/2, \quad h_{1y}(t) = 0, \tag{7}$$
$$h_{gx}(t) = \sin(2\pi t/\tau), \quad h_{gz}(t) = \cos(4\pi t/\tau),$$
$$g_x = g_z, \quad g_y = 0$$

for $-\tau_g \leqslant t \leqslant \tau_g$, where τ_g is the full width at half maximum of the Gaussian function and σ its standard deviation; the two-dimensional spatial response profile away from ($x = 0$, $z = 0$) exhibits peaks in perturbation along the x axis that are about half the size of those produced by the sombrero pulse. Indeed, this response, depicted in Fig. 3(a) for $g_x = 10^{-3}$ T/m, $\tau = 2$ ms, and a ^1H gyromagnetic ratio, bears some resemblance to an egg carton away from the origin. Note that the z gradient cycles twice during the Gaussian pulse period $\tau = 2\tau_g$, so the net gradient field vector describes a figure eight in the xz plane rather than a circle. The half height widths of the central portion of the response at $M_z = 0$ are approximately

$$\Delta x = 1.3\times 10^4/(\gamma g_x) \text{ m}$$

and

$$\Delta z = 1.8\times 10^4/(\gamma g_z) \text{ m},$$

with locations and amplitudes of the first few sidelobes and minima shown in the sectional profiles, Fig. 3(b).

C. Stalagmite pulse

The sensitivity of the profile to variations in the duration of the Gaussian waveform is illustrated in Fig. 4, where τ has been extended to $3\tau_g$. All other parameters in Eq. (7) are unchanged, except for h_{10} which decreases slightly to

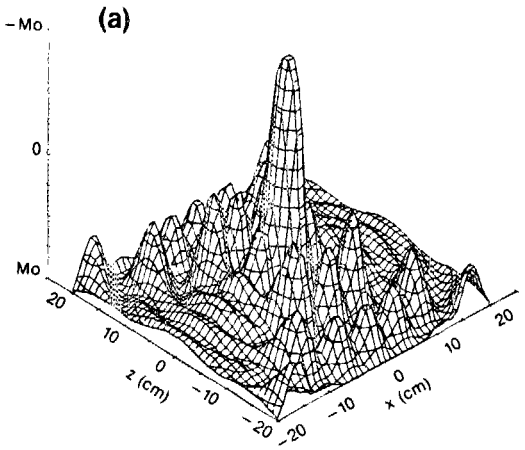

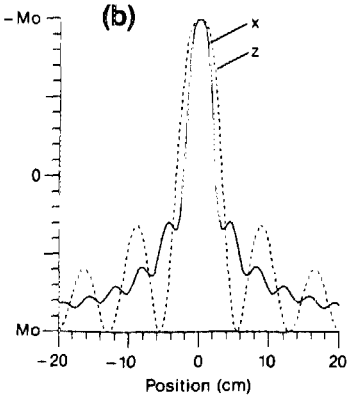

FIG. 3: Computed two-dimensional spatial response of a uniform distribution of nuclear spins subject to a two-dimensional selective NMR pulse defined by Eq. (7): (a) the egg-carton pulse. Vertical axes represent the z component of the nuclear magnetization in units of the equilibrium magnetization M_0 at each point r. Horizontal scales assume $g_x = g_z = 1.0$ mT/m, a ^1H gyromagnetic ratio, and $\tau = 2$ ms. (b) One-dimensional sectional profiles along the x axis (solid curve) and the z axis (dashed curve). The same spatial response for the magnitude of the transverse magnetization is obtained when the egg-carton pulse is used for refocusing spin echoes if the range of the vertical axis is rescaled to 0 to M_0 [or $M_0 \exp(-2T_E/T_2)$].

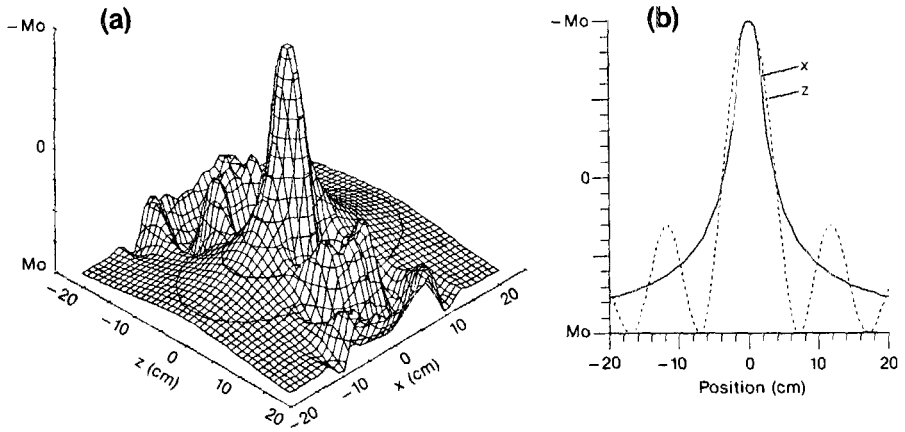

FIG. 4. (a) Computed two-dimensional spatial response of a uniform distribution of nuclear spins subject to a two dimensional selective NMR stalagmite pulse. Vertical axes represent the z component of the nuclear magnetization in units of the equilibrium magnetization M_0 at each point $\mathbf{r}$. Horizontal scales assume $g_x = 2g_z = 1.0$ mT/m, gyromagnetic ratio, and $\tau = 3$ ms. (b) One-dimensional sectional profiles along the x axis (solid curve) and the z axis (dashed curve). The same spatial response for the magnitude of the transverse magnetization is obtained when the stalagmite pulse is used for refocusing spin echoes if the range of the vertical axis is rescaled to 0 to M_0 [or $M_0 \exp(-2T_E/T_2)$].

$\tau/(1.06\gamma\tau_g)$, and g_z which has been reduced to $g_x/2$ to symmetrize the half widths of the central inversion lobe. The profile now appears smoother and the off-axis sidelobes have disappeared from the $z = 0$ plane [Fig. 4(b)]. The half height widths of the central portion of the response are

$$\Delta x = 2.0\times 10^4/(\gamma g_x) \text{ m}$$

and

$$\Delta z = 1.0\times 10^4/(\gamma g_z) \text{ m}.$$

D. Designer two-dimensional pulses

There are an infinite number of combinations of NMR pulse profiles and gradient modulations. Evaluation of a few of the more conventional types provided the following guidelines for designing two-dimensional selective inversion pulses:

(i) two-dimensional localization is not achieved when linearly dependent gradient modulations $h_{gx}(t)$, and $h_{gz}(t)$ are employed;

(ii) in the limit of large numbers of gradient modulation cycles completed in the pulse duration τ, the two-dimensional localization profiles excited by many NMR pulse types are comparable to the sombrero pulse;

(iii) the aspect ratio of localization profiles can usually be changed by varying either the relative gradient strengths g_x/g_z, etc., or the relative gradient modulation frequencies;

(iv) sinc (Ref. 9) and sech (Ref. 10) modulated NMR pulses do not produce two-dimensional localization except in the high-frequency gradient modulation limit noted above;

(v) two-dimensional localization is possible with gradient modulations that cycle less than once during τ;

(vi) other orthogonal gradient waveforms such as square and ramp functions also produce two-dimensional localization; and

(vii) as practical considerations, the selection of gradient waveforms and modulating frequencies is limited by the experimental response characteristics of the gradient coils and the amplifiers which drive them, while the pulse duration is limited by the requirement that $\tau \ll T_2^*$, where T_2^* is either the T_2 of the sample, or the inhomogeneously shortened transverse decay time of the sample in the absence of the reorienting gradients, or $(\pi\delta^*)^{-1}$, where δ^* is the width in frequency units of the chemical shift spectrum of the sample, whichever is smallest.

E. Two-dimensional spin echo refocusing pulses

The spatial response functions that result from the employment of the above rf and gradient pulse combinations as Hahn spin-echo refocusing π pulses can be derived by dividing the spin ensemble at $\mathbf{r}$ into a finite number n of spin packets that are each exposed to small variations ΔH_0^i in the main static magnetic field H_0. This field inhomogeneity is responsible for the dephasing of the transverse magnetization that the Hahn echo experiment is designed to overcome. Thus, for the ith spin packet, H_0 is replaced by $(H_0 + \Delta H_0^i)$ in Eq. (2), where the ΔH_0^i range from $-\Delta H_0^{\max}$ to $\Delta H_0^{\max}$ in equal increments of $2.\Delta H_0^{\max}/n$. The magnetization $\mathbf{M}^i$ of each packet is then allowed to evolve from an initial state $\mathbf{M}(t=0) = M_0\,\hat{\mathbf{y}}' = nM^i\hat{\mathbf{y}}'$ for a period $T_E = \pi/(\gamma\Delta H_0^{\max})$ in the absence of the excitation and gradient fields H_1 and H_g. During this period the different spin packets will have dephased by up to 2π in the rotating frame, as shown by Eq. (3) with $dt = T_E$. At time $t = T_E$, the NMR pulse and gradient fields are applied for a period τ and the magnetization computed for each packet by iterating Eq. (3) as was done for the inversion pulse. After a second evolution period T_E, the net magnetization $\mathbf{M}(\mathbf{r})$ is computed from the vector addition of the contributions from each spin packet. The transverse component of $\mathbf{M}(\mathbf{r})$ represents the spin-echo signal, and its two-dimensional spatial distribution is obtained by computing the result for an array of points (x,z) as before.

With $n = 24$, the two-dimensional sensitivity profiles of the transverse magnetization $M = (M_x^2 + M_y^2)^{1/2}$ for the sombrero, egg-carton, and stalagmite pulses employed as spin-echo refocusing pulses are the same as those obtained for inversion (Figs. 2–4) except that the vertical axes range from 0 to $+M_0$ (or strictly speaking 0 to $M_0 \exp(-2T_E/T_2)$ instead of $-M_0$ to $+M_0$. In these examples the phase of the transverse magnetization exhibits a small linear variation in the x dimension across the central localizing lobe. As in conventional one-dimensional selective excitation,[8,11]

this can be corrected with a constant refocusing x gradient pulse applied prior to data acquisition.

III. EXPERIMENT

To test the theoretical analysis, two-dimensional spatially selective inversion pulses were incorporated into a conventional slice selective two-dimensional Fourier transform spin-warp spin-echo NMR imaging pulse sequence,[15] as depicted in Fig. 5. The two-dimensional inversion pulses precede the initial $\pi/2$ NMR excitation pulse of the imaging sequence by a period $T_I \ll T_1$ of the nuclear spin system. The sequence is applied twice for each phase-encoding z gradient value, with the initial NMR inversion pulse alternately turned on and off. This causes those components of the detected NMR imaging signal that are perturbed by the initial pulse to be alternately inverted. Subtraction of these two NMR imaging signals yields, upon two-dimensional Fourier transform image reconstruction, an image of the two-dimensional excitation profile generated by the inversion pulse. Such images are directly comparable to the calculated profiles, Figs. 2–4, and can be compared with the response achieved in the absence of two-dimensional selective inversion simply by repeating the imaging experiment with the modulating gradients turned off during τ.

Experiments were performed on a 0.24-m-diam truncated cylinder of gelled 12-g/l agarose in 0.4-g/l $CuSO_4$ solution, and on a normal human volunteer using a 1.5 T 1 m bore NMR imaging/spectroscopy research system[16] operating at a 63.88 MHz ^1H resonance frequency. The agarose gel cylinder exhibited T_1 and T_2 values of 0.52 and 0.08 s, respectively, comparable to those of biological tissue.[17] A 6-mm-diam NMR-opaque peg occupied its cylindrical axis. Images consisted of 256×256 data points acquired with $T_I = 5$ ms and an imaging pulse sequence repetition period of 0.5 s. Sombrero, egg-carton, and stalagmite pulses were tested with τ values of 1, 2, and 3 ms, respectively ($\tau_g = 1$ ms), and modulating gradient amplitudes such that $g_x \sim 1$ mT/m throughout. Since these NMR pulse periods were comparable to the rise-time constants of the body-imaging gradient coils (~ 0.5 ms), the modulating gradients were turned on prior to commencement of the rf pulses and the relative phases adjusted to the correct relationship given by Eqs. (6) and (7). The application of such gradients in the absence of NMR pulses has no effect on the spin system if the transverse magnetization has already completely dephased. Also, to eliminate any spurious effects produced by eddy currents induced in the magnet structure by the modulating gradients, the latter were pulsed on for all applications of the imaging sequence, while only the NMR pulse was alternately switched on and off. The modulating gradients were left on for a short period after the inverting NMR pulse was complete, and the slice selection imaging gradient turned on during T_I to rapidly dephase any transverse magnetization excited by imperfect spin inversion.[18]

IV. RESULTS

^{1}H NMR images of the agarose cylinder without two-dimensional localization, and with the two-dimensional sombrero, egg-carton, and stalagmite selective inversion pulses, are shown in Fig. 6. The sensitivity profiles match the theoretical responses of Figs. 2–4. Measured values are compared to the theoretical values in Table I: they show good agreement although the central maxima and sidelobes are slightly depressed in the sombrero and stalagmite profiles.

The images in Fig. 7 demonstrate the effect of increasing both the rotating gradient amplitudes g_x and g_z using an egg-carton pulse in an imaging sequence applied to the human

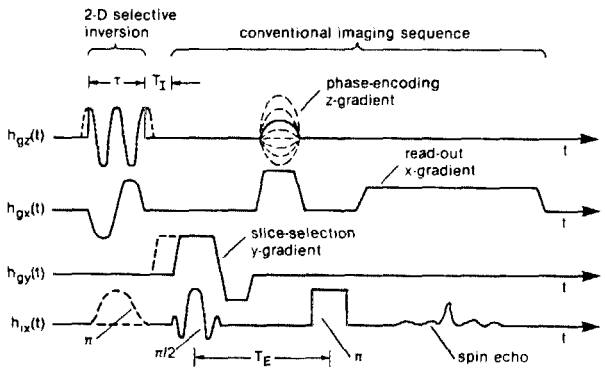

FIG. 5. NMR imaging pulse sequence timing diagram incorporating a two-dimensional inversion pulse prior to image slice selection. The selective inversion pulse waveforms illustrated correspond to an egg-carton pulse [Eq. (7)]. The initial π NMR pulse (dashed) on $h_{1x}(t)$ is alternately applied and not applied on consecutive applications of the sequence and the resulting spin-echo NMR signals acquired during the read-out gradient subtracted. Dashed lines on the initial $h_{gz}(t)$ and $h_{gy}(t)$ waveforms suggest practical additions to account for the rise time of the gradient system and/or to dephase any transverse magnetization generated by incomplete inversion. Images obtained with the h_{gx} and h_{gz} gradients turned off during τ serve as a control for comparing spatial selectivity.

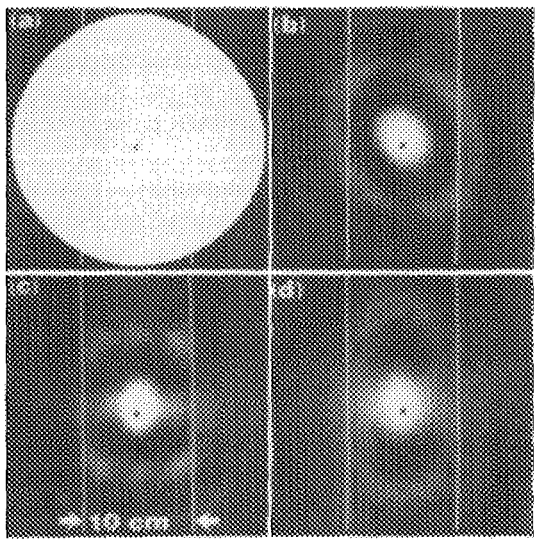

FIG. 6. ^{1}H NMR images of a cylinder of gelled agarose in $CuSO_4$-doped water obtained using the pulse sequence of Fig. 5: (a) with the two-dimensional localizing gradients turned off; (b) with a sombrero pulse; (c) with an egg-carton pulse; and (d) with a stalagmite pulse. The black spot at center is an NMR opaque peg. Parallel vertical line markers are separated by 10 cm. The images are oriented with the z axis vertical and the x axis horizontal. All NMR spectrometer and image display gains are kept constant throughout.

TABLE I. Comparison of theoretical and experimental intensity profiles.

Location on z axis	Theoretical intensities[a]	Measured image intensity[a]		
		sombrero	egg-carton	stalagmite
Center	1.0 ± 0.03	0.74 ± 0.09	1.07 ± 0.08	0.86 ± 0.09
1st minima	0.0	0.00 ± 0.01	0.01 ± 0.01	0.00 ± 0.01
1st sidelobe	0.35 ± 0.01	0.21 ± 0.06	0.37 ± 0.06	0.25 ± 0.06

[a] Relative to the image intensity measured at the center with the two-dimensional localizing gradients turned off (means $\pm$ S.D.).

head. Significant attenuation of eccentric NMR signal components in both dimensions is manifest, and the diameter of the central bright sensitive region is halved as the gradient strength is doubled.

V. DISCUSSION

The two-dimensional selective inversion pulses provide two-dimensional spatial localization and dramatic attenuation of NMR signals away from the axis of the rotating gradients as predicted. In imaging applications where it is desirable to image a small selected region of the sample with high spatial resolution, such attenuation significantly ameliorates artifacts derived from NMR signals external to the selected region. The imaging sequence of Fig. 5 is suitable for this selective volume high-resolution imaging if the conventional imaging gradients applied outside of τ and/or the data acquisition period are increased to accommodate the desired spatial resolution and restricted field of view for a given image array size. Rectangular image arrays can also be fairly accommodated by the elliptically symmetric responses that result from altering the aspect ratio by changing the gradient strengths and/or modulation frequencies. Note also that signal is lost from the sensitive region at a rate of $\exp(-T_I/T_1)$ due to recovery of the selectively inverted magnetization via T_1 relaxation during the interval prior to commencement of the imaging sequence.

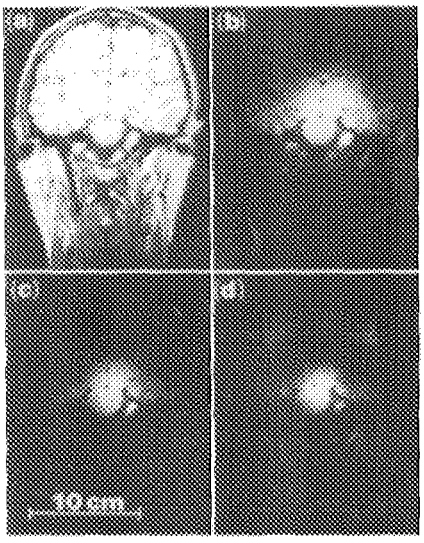

FIG. 7 (a) ^1H NMR images of the head of a normal human volunteer using the pulse sequence of Fig. 5 with the two-dimensional localizing gradients turned off, (b) with a $\tau = 2$ ms egg-carton pulse employing modulating gradient amplitudes $g_x = 0.5$ m T/m, (c) $g_x = 0.75$ mT/m, and (d) $g_x = 1.0$ mT/m. The imaging plane is oriented coronal at the level of the ears with the z axis vertical and x axis horizontal. The full width at half maximum diameter of the central bright region is about 10 cm in (b) and 5 cm in (d).

Use of the two-dimensional selective pulses for spin-echo refocusing in NMR imaging just requires the substitution of a two-dimensional pulse for the conventional π pulse depicted in Fig. 5. Inclusion of an x gradient rephasing pulse to compensate for phase variations in the localized transverse magnetization following the π spin echo pulse is not, in general, necessary for high-resolution restricted field of view imaging, where the phase variations across individual image picture elements are typically negligible. It should, however, be included for spectroscopy. For both imaging and spectroscopy applications involving spin-echo refocusing, sequences are not repeated twice with and without the two-dimensional π pulse: localization is achieved in a single sweep. In these applications, the spin-echo signal is lost from the localized volume at the usual rate, $\exp(-2T_E/T_2)$, due to T_2 relaxation.

When the location of the region of interest and the cylindrical axis of the rotating gradients do not coincide, they must be moved. While the physical relocation of either the gradient coil set or the sample is not impossible, it is often impractical due to space and weight considerations. Simply offsetting the NMR frequency in a single sideband transmitter, as is done for one-dimensional selective excitation, in general spreads the selected volume about the xz plane rather than moving it, although more sophisticated frequency modulations of the NMR pulse waveforms may prove effective. Otherwise, the same solution used for moving the sensitive region in the early sensitive point imaging technique[12-14] is applicable: a linear change in the ratio of the currents in the two halves of each gradient coil set linearly advances the location of the cylindrical axis of the rotating gradient, moving the selected volume. Given access to the inputs of each gradient coil half, the ratio of the gradient currents can be altered with motor-driven potentiometers,[12] multiplying digital-to-analog circuitry,[19] or directly via the imaging systems computer interface and gradient amplifiers.

Improvements in the sensitivity profile may be necessary if the two-dimensional selective pulses are used to provide two-dimensional spatial localization in the absence of additional spatial localization procedures. In such cases, the detected NMR signal represents the total integrated contributions from the sample, so that the NMR signals from the sidelobes, while low in amplitude, can, when integrated, easily swamp those from the central inversion lobe as the relative sample size is increased. The same problem has been noted in sensitive point NMR imaging.[20] Unfortunately, optimizing the sensitivity profile to eliminate the troublesome sidelobes involves a tedious trial-and-error application of the theory using different input functions, a problem all too commonly encountered when solving complex differential equations. Nevertheless, an optimization procedure seeking combinations of pulse modulation functions that minimize side lobe contributions is presently underway.

Meanwhile, one simple means of providing adequate at-

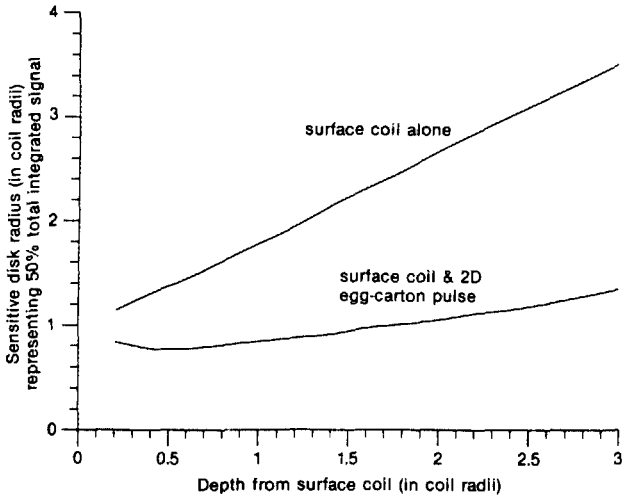

FIG. 8. The radius of the sensitive volume, assumed circular, representing 50% of the total integrated signal in planes oriented parallel to the surface coil as a function of depth along the coil axis. The two curves illustrate the result with the surface coil alone (above), and with a two-dimensional egg-carton pulse with central half-height diameter equal to that of the surface coil. All dimensions are in coil radii. The curve was obtained by iterative integration of the sensitivity profiles until they represented 50% of the total signal at each depth assuming a homogeneous sample.

tenuation of the sidelobes is to use surface coils for detecting the NMR signals. In phosphorus (^{31}P), carbon (^{13}C), and ^{1}H metabolite localized NMR spectroscopy where surface coils are regularly employed because of their substantial advantage in signal-to-noise ratio,[5] the two-dimensional selective pulses could be used to provide spatial localization to a disk-shaped volume parallel to the surface coil. Thus, if a surface detection coil is combined with an egg-carton pulse of spatial half-height width equal to the surface coil diameter, the radius of the sensitive disk representing 50% of the total integrated signal in the plane of the disk is both independent of the sample size and approximately independent of depth from the surface coil (Fig. 8). In contrast, the sensitive disk radius representing 50% of the integrated signal diverges with depth when surface coil localization alone is employed.[21]

In such surface coil spectroscopy applications, spatial localization along the third dimension parallel to the axis of the surface coil and the cylindrical axis of the modulating gradients can be achieved by subsequent or prior application of the depth-resolved surface coil spectroscopy sequence (DRESS),[3] the slice interleaved DRESS (SLITDRESS) sequence,[22] or the rotating frame zeugmatography sequence,[23] yielding complete three-dimensional localization of NMR spectra. In the former case of DRESS or SLITDRESS sequences combined with a two-dimensional selective inversion pulse, three-dimensional localization is complete in just two applications of the sequence, with and without inversion, compared with the eight applications required using conventional selective inversion alone.[4] In the acronymonial tradition of NMR, we shall denote the new three-dimensional localized spectroscopy sequence subsuming the DRESS and SLITDRESS techniques by the acronym PROGRESS for point-resolved rotating gradient surface coil spectroscopy.

Note added in proof. Since submission of this manuscript, the PROGRESS localized spectroscopy sequence incorporating an egg-carton pulse has been successfully used to acquire ^{31}P NMR spectra *in vivo*.[24] The application of a simulated annealing computer optimization procedure to the problem of designing pulses with minimal sidelobe contributions has yielded several promising solutions.[25]

ACKNOWLEDGMENTS

We thank W. M. Leue for programming the two-dimensional pulse sequence into our research NMR imaging machine, and J. Piel for volunteering for the human studies.

[1] P. Mansfield and P. G. Morris, *NMR Imaging in Biomedicine* (Academic, New York, 1982), pp. 32–114.
[2] P. A. Bottomley, Rev. Sci. Instrum. **53**, 1319 (1982).
[3] P. A. Bottomley, T. H. Foster, and R. D. Darrow, J. Magn. Reson. **59**, 338 (1984).
[4] R. J. Ordidge, A. Connelly, and J. A. B. Lohman, J. Magn. Reson. **66**, 283 (1986).
[5] P. A. Bottomley, *Medical Magnetic Resonance Imaging and Spectroscopy*, edited by T. F. Budinger and A. R. Margulis (Society of Magnetic Resonance in Medicine, Berkeley, CA, 1986), pp. 81–95.
[6] P. C. Lauterbur, C. S. Dulcey, C. M. Lai, M. A. Feiler, W. V. House, D. Kramer, C. N. Chen, and R. Dias, in *Proceedings of the 18th Congress Ampere*, Nottingham 1974, edited by P. S. Allen, E. R. Andrew, and C. A. Bates (North-Holland, Amsterdam, 1975), pp. 27–29.
[7] A. N. Garroway, P. K. Grannell, and P. Mansfield, J. Phys. C **7**, L457 (1974).
[8] R. J. Sutherland and J. M. S. Hutchison, J. Phys. E **11**, 79 (1978).
[9] P. Mansfield, A. A. Maudsley, and T. Baines, J. Phys. E **9**, 271 (1976).
[10] M. S. Silver, R. I. Joseph, C. N. Chen, V. J. Sank, and D. I. Hoult, Nature (London) **310**, 681 (1984).
[11] D. I. Hoult, J. Magn. Reson. **26**, 165 (1977).
[12] W. S. Hinshaw, J. Appl. Phys. **47**, 3709 (1976).
[13] W. S. Hinshaw, P. A. Bottomley, and G. N. Holland, Nature (London) **270**, 722 (1977).
[14] P. A. Bottomley, J. Magn. Reson. **50**, 335 (1982).
[15] W. A. Edelstein and P. A. Bottomley, U.S. patent No. 4,471,306 (issued Sept. 11, 1984).
[16] P. A. Bottomley, H. R. Hart, W. A. Edelstein, J. F. Schenck, L. S. Smith, W. M. Leue, O. M. Mueller, and R. W. Redington, Radiol. **150**, 441 (1984).
[17] P. A. Bottomley, T. H. Foster, R. E. Argersinger, and L. M. Pfeifer, Med. Phys. **11**, 425 (1984).
[18] P. A. Bottomley and W. A. Edelstein, U.S. patent No. 4,484,138 (issued Nov. 20, 1984).
[19] P. A. Bottomley, J. Phys. E **14**, 1081 (1981); W. S. Hinshaw (private communications, 1975–1978).
[20] F. T. Meiere and F. C. Thatcher, J. Appl. Phys. **50**, 4491 (1979).
[21] P. A. Bottomley, Ann. NY Acad. Sci. **508** (in press 1987).
[22] P. A. Bottomley, L. S. Smith, W. M. Leue, and C. Charles, J. Magn. Reson. **64**, 347 (1985).
[23] S. J. Cox and P. Styles, J. Magn. Reson. **40**, 209 (1980).
[24] P. A. Bottomley and C. J. Hardy, J. Magn. Reson. **74**, 550 (1987).
[25] C. J. Hardy, P. A. Bottomley, M. O'Donnell, and P. B. Roemer, in *Proceedings of the 6th Annual Meeting of the Society of Magnetic Resonance in Medicine*, New York, 1987 (Society of Magnetic Resonance in Medicine, Berkeley, CA, 1987), Vol. 1, p. 479; J. Magn. Reson. (in press).